Polymer 149 (2018) 85–95

Contents lists available at ScienceDirect

Polymer

journal homepage: www.elsevier.com/locate/polymer

Design and synthesis of 2D A_1-π-A_2 copolymers impact on fullerene network for efficient polymer solar cells

Sung Jae Jeon, Tae Ho Lee, Yong Woon Han, Doo Kyung Moon*

Department of Materials Chemistry and Engineering, Konkuk University, 1 Hwayang-dong, Gwangjin-gu, Seoul, 143-701, South Korea

ARTICLE INFO

Article history:
Received 15 December 2017
Received in revised form
2 April 2018
Accepted 10 April 2018
Available online 11 April 2018

Keywords:
Polymer solar cells (PSCs)
Fullerene inter-chain packing
Two-dimensional (2D)

ABSTRACT

A new building block of two-dimensional (2D) A_1-π-A_2 copolymers for P(dDTPz-ID) and P(dDTPz-DTBT) was designed and synthesized. Their structures have two strong acceptor units (isoindigo and benzothiadiazole derivatives) in the backbone, respectively. It displayed a benefit of A_1-A_2 building blocks, which is complementary and broad light absorption from 300 to 750 nm due to acceptors with different withdrawing strengths. Also, the introduction of dangling-thiophene, π unit allowed the formation of 2D-strcuture, which and led to effective and inter-chain packing of $PC_{71}BM$ for both copolymers. Two copolymers exhibited enhanced π-π stacking properties and had predominant face-on structure, which was confirmed by XRD. We also reviewed the optical, electrochemical, morphological, charge transport properties and performance compared with A_1-A_2 copolymers for P(DTPz-ID) and P(DTPz-DTBT), respectively. The inverted device fabricated with optimized condition for P(dDTPz-DTBT) showed efficient charge transport from enhanced energy alignment, high V_{oc} and dipole moment and fine morphology, and thus obtained 5.0% of best power conversion efficiency (PCE).

1. Introduction

Polymer solar cells (PSCs) based on bulk-heterojunction (BHJ), composed of electron rich donor (D)-electron deficient acceptor (A) polymer as donor and fullerene derivative as acceptor, can be used to produce flexible devices and large area by solution-process. Therefore, it is interest in the research field of clean and renewable energy [1–3]. The greater part of BHJ structures with high performance fullerene PSCs forms bicontinuous donor/acceptor interfaces and undergo efficient exciton dissociation [4]. However, it is indeed difficult to reach fine inter-chain packing between the bulky fullerene acceptor and polymer donor [5,6]. To increase the efficient fullerene inter-chain packing between polymer chains, structural modifications such as backbone manipulations [7–11], side-chain engineering [12,13], as well as incorporation of newly developed building blocks [14–16] are needed to be conducted on the donor polymer. Recently, new building blocks through the side chain engineering were demonstrated based on polythiophene (PT) derivatives that achieve power conversion efficiencies (PCEs) of 7–11% in fullerene PSCs [16–18].

There have been reports on two-dimensional (2D)-building block concepts including D-π-A and A-π-D types, which are not typical D-A building blocks as high performance conjugated polymer donor for PSCs [19–21]. The inserted π-conjugated bridge between D-A frameworks provide a stero-structure on the polymer backbone, and have crucial effect on photophysical, electrochemical, charge transport, and photovoltaic properties of the donor polymer [22]. In particular, since the polymer has 2D-conjugated architecture, it can have close contact with fullerene acceptors, and thus efficient charge separation and transfer at the interface can be expected [23].

Most D-A polymers have one chromophore unit to design low band gap donor. Thus, The introduction of two chromophores resulted in the development of D-A_1-D-A_2 or A_1-A_2 building blocks that can extend the absorption band in long wavelength region [24–26]. Ergang Wang group have reported over 7.0% PCE which has shown the benefits of A_1-A_2 concept, compared with conventional D-A polymers [24]. The quinoxaline and iosoindigo composed of A_1-A_2 polymers were used as the two electron-deficient units. It was shown that alternating copolymers based on the regio-regular structure forms π-stacking structure, providing higher carrier mobility compared to random copolymers with two acceptor units [24,25].

Improved by two strategies of 2D-conjugated concept and A_1-A_2

* Corresponding author.
E-mail address: dkmoon@konkuk.ac.kr (D.K. Moon).

https://doi.org/10.1016/j.polymer.2018.04.032
0032-3861/

building block in the main backbone of conjugated copolymers, we suggest a new concept with A_1-π-A_2 building block in this study. Our concept was designed to allow effective inter-chain packing of fullerene acceptors to polymer backbone, and the introduction of acceptors with two different electron-withdrawing strengths is expected to result in complementary and broad absorption bands of 2D A_1-π-A_2 copolymers.

For A_1, 11,12-bis(octyloxy)-10,13-di(thiophen-2-yl)dibenzo[a,c] phenazine (DTPz) [27], which is a medium acceptor with high planarity that has 450–550 nm intermolecular charge transfer (ICT) effect in silole-based D-A polymers [28], was selected. Next, for A_2, di(2-octyldodecyl)isoindigo (ID), which is a strong acceptor with planar structure that has 600–750 nm of ICT effect in alkylidene-based D-A polymers [29]; and 5,6-bis(octyloxy)-4,7-di(thiophen-2-yl)benzo[c] [1,2,5]thiadiazole (DTBT) which has 550–650 nm of ICT effect in benzodithiophene-based D-A polymers [3], were selected. Lastly, for π-conjugated bridge between A_1 and A_2, dangling (as called d) thiophene was introduced to enhance charge carrier mobility and to provide stero-2D-conjugation point.

The two types of originally synthesized A_1-π-A_2 copolymers are named P(dDTPz-ID) and P(dDTPz-DTBT), and complementary and broad light absorption bands were obtained. We also synthesized and characterized A_1-A_2 copolymers for P(DTPz-ID) and P(DTPz-DTBT) to prove their effects of A_1-π-A_2. All copolymers showed face-on orientation; P(dDTPz-DTBT) most effectively inter-chain packing on $PC_{71}BM$ among the copolymers and showed a maximum of 5.0% PCE due to its efficient charge transport. This new design concept for donor copolymer with A_1-π-A_2 building block is expected to be the instructive guide in developing two-dimensional copolymer donors in PSCs.

2. Experimental section

2.1. Instruments and characterization

Unless otherwise specified, all reactions were performed under a nitrogen atmosphere. The solvents were dried using the standard procedures. All column chromatography was performed with silica gel (230–400 mesh, Merck) as the stationary phase. ^{1}H NMR spectrum were collected by a Bruker ARX 400 spectrometer using solutions in $CDCl_3$ with chemical concentrations recorded in ppm units using TMS as the internal standard. The elemental analyses were measured with an EA1112 apparatus using a CE Instrument. The electronic absorption spectra were measured in diluted chloroform solution and thin films on ITO glass using an HP Agilent 8453 UV–Vis spectrophotometer. The cyclic voltammetry (CV) curves were obtained using a Zahner IM6eX electrochemical workstation with a 0.1 M acetonitrile (purged with nitrogen for 20 min) solution containing tetrabutyl ammonium hexafluorophosphate (Bu_4NPF_6) as the electrolyte at a constant scan rate of 50 mV/s. ITO, a Pt wire, and silver/silver chloride [Ag in 0.1 MKCl] were used as the working, counter, and reference electrodes, respectively. The electrochemical potential was calibrated against Fc/Fc+. The high occupied molecular orbital (HOMO) levels of the polymers were determined using the oxidation onset value. The onset potentials are the values obtained from the intersection of the two tangents drawn at the rising current and the baseline changing current of the CV curves. Thermogravimetric analysis (TGA) measurements were performed on a NETZSCH TG 209 F3 thermogravimetric analyzer. All gel permeation chromatography (GPC) analyses were performed using chloroform as an eluent and a polystyrene standard as a reference. XRD patterns were obtained using a Smart Lab 3 kW (40 kV 30 mA, Cu target, wavelength: 1.541871 Å) instrument of Rigaku, Japan. Topographic images of the active layers were obtained through atomic force microscopy (AFM) in a tapping mode under ambient conditions using an XE-100 instrument. Theoretical analyses were performed using density functional theory (DFT), as approximated by the hybrid B3LYP functional and employing the 6-31G(d) basis set in Gaussian 09.

2.2. Fabrication and characterization of PSCs

All the BHJ photovoltaics cells were prepared using the following device fabrication procedure. Indium tin oxide (ITO) glass (10 X/sq, Samsung corning) was sequentially sonicated in detergent (Alconox in deionized water, 10%), acetone, isopropyl alcohol, and deionized water for a period of 20 min. The moisture was thoroughly removed with a N_2 gas flow. To ensure the complete removal of the remaining water, the ITO glass was heated on a hot plate for 10 min at 100 °C. For the hydrophilic treatment of the ITO glass surface, the glass was cleaned for 10 min in a UVO cleaner. Zinc oxide (ZnO) was passed through a poly(tetrafluoroethylene) (PTFE) 0.45 μm filter before being deposited on ITO at a thickness of ca. 30 nm by spin-coating at 4000 rpm in air, and then dried for 30 min at 120 °C inside a glove box. Composite solutions of the polymers and $PC_{71}BM$ were prepared using chlorobenzene (CB) with 1% 1,8-diiodooctane (DIO). The solutions were filtered through a PTFE 0.45 μm filter and then spin-coated (700–5000 rpm, 30 s) on top of the ZnO layer. The inverted device fabrication was completed by depositing thin layers of ZnO (10 nm), MoO_3 (2 nm) and Ag (100 nm) at pressures of less than 1026 Torr. The active area of the device was 0.07–0.12 cm^2. The output photocurrent was adjusted to match the photocurrent of the Si reference cell to obtain a power density of 100 mW cm^{-2}.

2.3. Polymerization

Scheme 1 outlines the synthetic route to the monomers and the polymers. The detailed synthetic procedures and characterization results for the monomers (M0, M1, M2 and M3) are presented in the Supporting Information (SI, see Figs. S1–S10).

2.3.1. P(DTPz-ID)

M0 (142.9 mg, 0.15 mmol), M2 (161.3 mg, 0.15 mmol), $Pd(PPh_3)_4$ (6.83 mg) 0.032 mmol) were dissolved in anhydrous toluene (10 mL). The flask was degassed and refilled with nitrogen gas twice, and then 2 M aqueous K_2CO_3 solution (1.38 g, 10 mmol in H_2O 5 mL) and Aliquat 336 (2 drops) was added to the mixture. The flask was degassed and refilled twice. The polymerization mixture was stirred at 95 °C for 48 h, and a few drops of 2-bromothiophene were added. After 4 h, a few drops of 2-tributylstannyl thiophene were also added for 4 h. The reaction mixture was cooled to room temperature and poured into methanol. The precipitate was filtered and purified with methanol (24 h), acetone (24 h), hexane (18 h), ethyl acetate (18 h) and chloroform (2 h) in a Soxhlet apparatus. The polymer of the chloroform fraction was filtered with celite and re-precipitated in methanol. Finally, the polymer was collected as a dark black solid (Yield: 104 mg, 40%) ^{1}H NMR (400 MHz; $CDCl_3$; Me_4Si), δ (ppm): 9.49 (m, 4H), 8.62–8.52 (m, 2H), 8.24–8.15 (m, 2H), 8.08–8.00 (m, 2H), 7.88–7.81 (m, 2H), 7.67–7.52 (m, 2H), 7.46–7.29 (m, 4H), 4.18–4.03 (m, 4H), 3.75–3.45 (m, 4H), 2.29–1.80 (m, 4H), 1.42–0.95 (m, 80H), 0.91–0.80 (m, 18H). Calculated analysis for $C_{106}H_{136}N_4O_4S_2$ (%): C, 78.90; H, 9.00; N, 3.68; O, 4.20; S, 4.21; Elemental analysis (EA), Found (%): C 78.60; H, 9.44; N, 3.20; O, 3.81; S, 3.12.

2.3.2. P(dDTPz-ID)

M2 (145 mg, 0.15 mmol), M2 (161.3 mg, 0.15 mmol), $Pd(PPh_3)_4$ (6.83 mg) 0.032 mmol) were dissolved in anhydrous toluene (11 mL). The flask was degassed and refilled with nitrogen gas

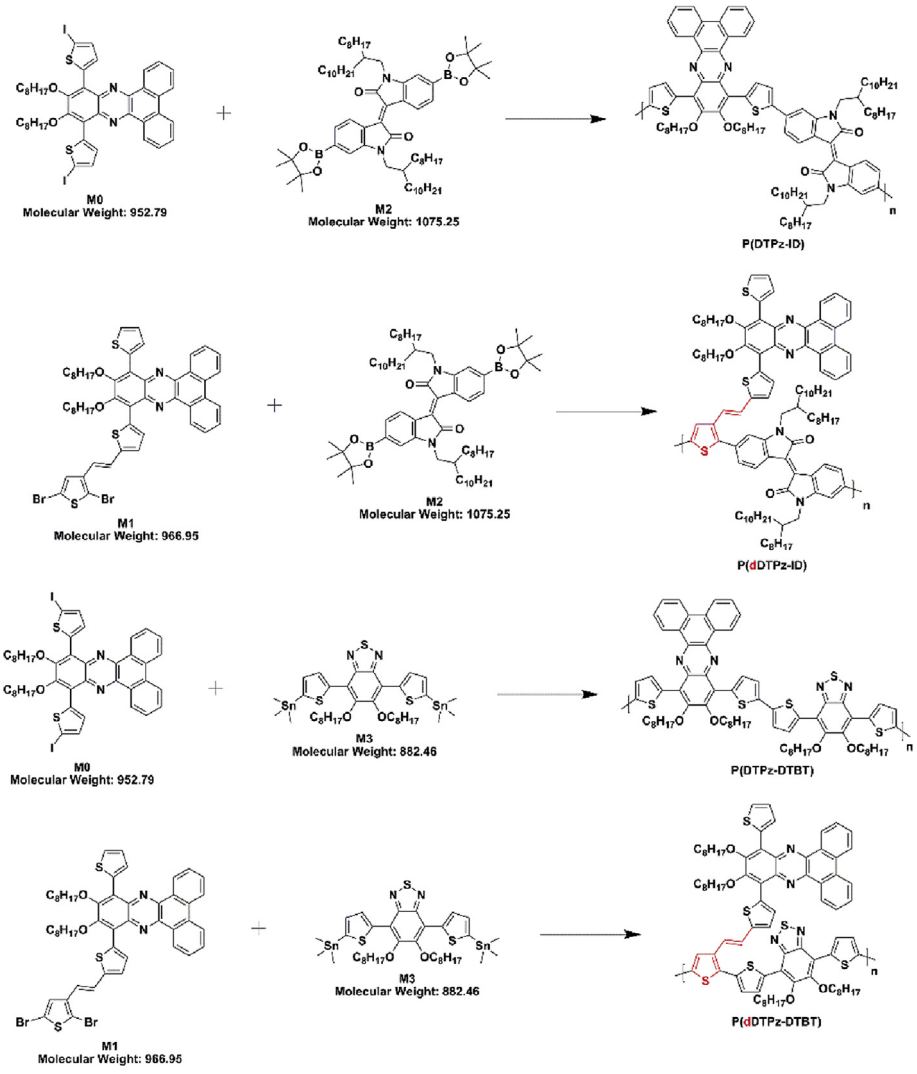

Scheme 1. Synthesis routes of polymers.

twice, and then 2 M aqueous K_2CO_3 solution (1.38 g, 10 mmol in H_2O 5 mL) and Aliquat 336 (2 drops) was added to the mixture. The flask was degassed and refilled twice. The polymerization mixture was stirred at 95 °C for 48 h, and a few drops of 2-bromothiophene were added. After 4 h, a few drops of 2-tributylstannyl thiophene were also added for 4 h. The reaction mixture was cooled to room temperature and poured into methanol. The precipitate was filtered and purified with methanol (24 h), acetone (24 h), hexane (18 h), ethyl acetate (18 h) and chloroform (2 h) in a Soxhlet apparatus. The polymer of the chloroform fraction was filtered with celite and re-precipitated in methanol. Finally, the polymer was collected as a dark black solid (Yield: 60 mg, 25%) ^{1}H NMR (400 MHz; $CDCl_3$; Me_4Si), δ (ppm): 9.38–9.20 (m, 6H), 8.94–8.85 (m, 2H), 8.32–8.24 (m, 2H), 8.11–8.00 (m, 2H), 7.61–7.58 (m, 2H), 7.49–7.46 (m, 4H), 7.11–7.02 (m, 4H), 4.18–4.03 (m, 4H), 3.75–3.45 (m, 4H), 2.05–1.80 (m, 4H), 1.42–0.95 (m, 80H), 0.91–0.80 (m, 18H). Calculated analysis for $C_{106}H_{140}N_4O_4S_3$ (%): C, 78.08; H, 8.65; N, 3.44; O, 3.93; S, 5.90; Elemental analysis (EA), Found (%): C 77.52; H, 8.57; N, 3.12; O, 3.65; S, 4.70.

2.3.3. P(DTPz-DTBT)

M0 (142.9 mg, 0.15 mmol), M3 (132.4 mg, 0.15 mmol) were dissolved in anhydrous toluene (5 mL). The flask was degassed and refilled with nitrogen gas twice, and then $Pd_2(dba_3)$ (5.48 mg) and p(o-tol)$_3$ (7.3 mg) was added to the mixture. The flask was degassed and refilled twice. The polymerization mixture was stirred at 100 °C for 48 h, and a few drops of 2-bromothiophene were added. After 4 h, a few drops of 2-tributylstannyl thiophene were also added for 4 h. The reaction mixture was cooled to room temperature and poured into methanol. The precipitate was filtered and purified with methanol (24 h), acetone (24 h), hexane (24 h), ethyl acetate (24 h) and chloroform (3 h) in a Soxhlet apparatus. The polymer of the chloroform fraction was filtered with celite and re-precipitated in methanol. Finally, the polymer was collected as a dark violet solid (Yield: 65 mg, 37%) ^{1}H NMR (400 MHz; $CDCl_3$; Me_4Si), δ (ppm): 9.50–9.45 (m, 2H), 9.35–9.33 (m, 2H), 8.53–8.49 (m, 2H), 8.21–8.18 (m, 2H), 7.78–7.68 (m, 2H), 7.63–7.30 (m, 6H), 4.25–4.08 (m, 8H), 1.93–1.58 (m, 8H), 1.32–1.12 (m, 40H), 1.05–0.90 (m, 12H). Calculated analysis for $C_{74}H_{86}N_4O_4S_5$ (%): C, 70.77; H, 6.90; N, 4.46; O, 5.10; S, 12.77; Elemental analysis (EA), Found (%): C 70.51; H, 7.35; N, 3.99; O, 4.25; S, 11.50.

2.3.4. P(dDTPz-DTBT)

M2 (145 mg, 0.15 mmol), M3 (132.4 mg, 0.15 mmol) were dissolved in anhydrous toluene (6 mL). The flask was degassed and refilled with nitrogen gas twice, and then $Pd_2(dba_3)$ (5.48 mg) and

p(o-tol)$_3$ (7.3 mg) was added to the mixture. The flask was degassed and refilled twice. The polymerization mixture was stirred at 100 °C for 48 h, and a few drops of 2-bromothiophene were added. After 4 h, a few drops of 2-tributylstannyl thiophene were also added for 4 h. The reaction mixture was cooled to room temperature and poured into methanol. The precipitate was filtered and purified with methanol (24 h), acetone (24 h), hexane (24 h), ethyl acetate (24 h) and chloroform (3 h) in a Soxhlet apparatus. The polymer of the chloroform fraction was filtered with celite and re-precipitated in methanol. Finally, the polymer was collected as a dark violet solid (Yield: 95 mg, 46%) ^{1}H NMR (400 MHz; $CDCl_3$; Me_4Si), δ (ppm): 9.46–9.41 (m, 2H), 9.35–9.33 (m, 2H), 9.25–9.23 (m, 2H), 8.66–8.41 (m, 2H), 8.27–8.20 (m, 2H), 8.10–8.07 (m, 2H), 7.68–7.64 (m, 2H), 7.44–7.41 (m, 2H), 7.31–7.30 (m, 2H), 7.14–7.11 (m, 2H) 4.16–4.07 (m, 6H), 3.78–3.53 (m, 2H), 2.07–2.01 (m, 1H), 1.86–1.80 (m, 3H), 1.43–1.16 (m, 44H), 0.99–0.74 (m, 12H). Calculated analysis for $C_{80}H_{90}N_4O_4S_6$ (%): C, 70.44; H, 6.65; N, 4.11; O, 4.69; S, 14.10; Elemental analysis (EA), Found (%): C 70.02; H, 6.33; N, 4.09; O, 4.21; S, 14.13.

3. Results and discussion

3.1. Synthesis and characterization

The synthesized polymers exhibit good solubility in common organic solvents such as tetrahydrofuran, dichloromethane, chloroform, chlorobenzene, and o-DCB, rendering them good candidates for the fabrication of organic semiconductors [30]. The measured molecular weights and thermal properties of polymers are summarized in Table 1 and Fig. S11. P(DTPz-ID), P(dDTPz-ID), P(DTPz-DTBT) and P(dDTPz-DTBT) have weight-average molecular weight (M_w) of 65.9, 59.8, 48.8 and 51.1 kDa, and broad polydispersity index (PDI) 2.71, 3.96, 2.65 and 2.62, respectively. These data were determined by GPC, calibrated by polystyrene standards using chloroform as an eluent at RT. The thermal stability of conjugated polymers is very important for their application in optoelectronic device [20]. The P(DTPz-ID), P(dDTPz-ID), P(DTPz-DTBT) and P(dDTPz-DTBT) confirmed high thermal stability with decomposition temperature (T_d, 5% weight loss) in a 353, 366, 328 and 340 °C through TGA under a nitrogen atmosphere at a heating rate of 20 °C min^{-1}.

Table 1
Physical and thermal properties of polymers.

Polymer	M_n[a] [kDa]	M_w[a] [kDa]	PDI[a]	T_d[b] [°C]
P(DTPz-ID)	24.3	65.9	2.71	353
P(dDTPz-ID)	15.1	59.8	3.96	366
P(DTPz-DTBT)	18.4	48.8	2.65	328
P(dDTPz-DTBT)	19.5	51.1	2.62	340

[a] Determined by GPC in chloroform using polystyrene standards.
[b] Temperature resulting in 5% weight loss based on the initial weight.

3.2. Optical and electrochemical properties

To examine effects of copolymers with A_1-A_2 and 2D A_1-π-A_2 building blocks on the optical properties, UV–vis absorption spectra of copolymers in chloroform solutions and thin films are shown in Fig. 1. Fig. 2 shows the cyclic voltammograms of copolymers films. The corresponding optical and electrochemical properties of the copolymers are summarized in Table 2. Fig. 1 (a) shows average molar absorption coefficients of copolymers measured in different solution concentrations, respectively. Both polymers of P(DTPz-ID) and P(dDTPz-ID) showed three absorption peaks, the first peak of maximum 347 nm and 319 nm is the π-π* absorption of D-thiophene ID or/and DTPz [31]. The second absorption peak of maximum 416 nm and 392 nm for P(DTPz-ID) and P(dDTPz-ID) is due to a delocalized excitonic π-π* transition of conjugated polymer backbone [32]. In particular, the third peak of 450–750 nm for both polymers showed broad absorption peak which is due to strong ICT interaction between the two acceptors, respectively (DTPz and ID) [25]. However, the ICT effect of P(DTPz-ID) and P(dDTPz-ID) looks difference of intensity and waveform in long wavelength region. By introduced D-thiophene unit in A_1-A_2 polymer backbone, blue shift was observed. It was due to the backbone twist between A_1 and A_2 in P(dDTPz-ID) [33]. Also, It affected that molar absorption coefficients (ε) which were calculated using Beer-lambert ($A = \varepsilon bc$). The results of P(DTPz-ID) and P(dDTPz-ID) were 40,075 M^{-1} cm^{-1}, 26,358 M^{-1} cm^{-1}, 43,970 M^{-1} cm^{-1} for 347 nm, 416 nm, 656 nm and 41,175 M^{-1} cm^{-1}, 34,612 M^{-1} cm^{-1}, 21,700 M^{-1} cm^{-1} for 319 nm, 392 nm, 619 nm, respectively. Consequently, P(DTPz-ID) has better optical properties than P(dDTPz-ID) in solution states.

P(DTPz-DTBT) and P(dDTPz-DTBT) also showed three distinct absorption peaks, first and second peaks showed maximum absorption peaks at 342 nm, 398 nm and 319 nm, 392 nm respectively. P(DTPz-DTBT) showed stronger third peak at 581 nm than those of P(dDTPz-DTBT). It was identical to previous trends of P(DTPz-ID) and P(dDTPz-ID). The ε values of P(DTPz-DTBT) and P(dDTPz-DTBT) were calculated to be 31,188 M^{-1} cm^{-1}, 36,666 M^{-1} cm^{-1}, 36,885 M^{-1} cm^{-1} for 342 nm, 398 nm, 581 nm and 55,114 M^{-1} cm^{-1}, 56,096 M^{-1} cm^{-1}, 40,681 M^{-1} cm^{-1} for 319 nm, 392 nm, 535 nm, respectively. It seems that P(dDTPz-DTBT) has better optical properties than P(DTPz-DTBT). However, P(dDTPz-DTBT), The third peak at 450–650 nm showed narrower absorption peak compared to the ICT effect of P(dDTPz-ID), which is due to limitations in light absorption in long wavelength region since DTBT has weaker electron affinity compared to ID. Even if P(dDTPz-DTBT) has weak absorption in long wavelength region, it has higher effect in whole photon energy absorption compared to P(dDTPz-ID).

At Fig. 1 (b) and (c) show normalized UV–vis spectra of A_1-A_2 and 2D A_1-π-A_2 copolymers in solution versus film. All copolymers have high aggregation to solid state and showed little change in λ_{max} in short wavelength range. λ_{max} of P(dDTPz-ID) had slightly

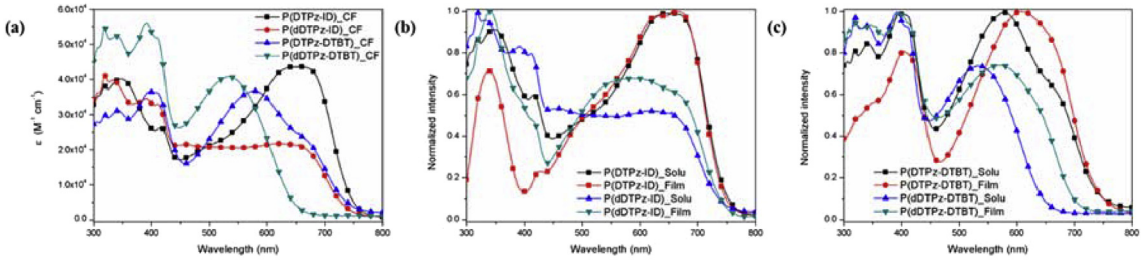

Fig. 1. (a) UV–visible absorption coefficients in solutions and (b, c) spectra in solutions versus thin films for polymers.

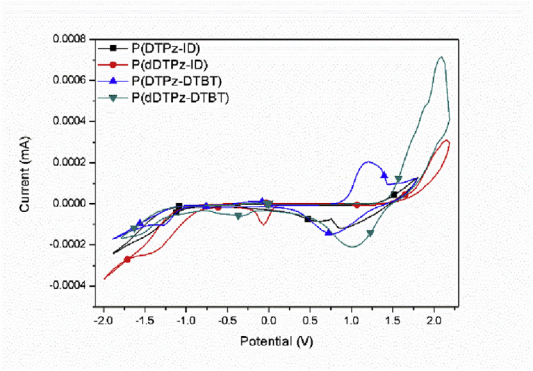

Fig. 2. Cyclic voltammograms of polymers.

blue-shift from 656 nm to 666 nm, but cases of P(DTPz-ID), P(DTPz-DTBT) and P(dDTPz-DTBT) had red-shift from 535 nm to 574 nm, 581 nm–608 nm and 535 nm–574 nm in long wavelength range, respectively. However, The low optical band gap (E_g^{opt}) of all copolymers, obtained from the onset of the absorption spectra in film, was estimated to be 1.63 eV of P(DTPz-ID), 1.67 eV of P(dDTPz-ID), 1.65 eV of P(DTPz-DTBT) and 1.78 eV of P(dDTPz-DTBT). In particular, copolymers based on DTBT showed stronger intermolecular interaction between polymer chains in film formation compared to polymers with ID.

The electrochemical behavior of the A_1-A_2 and 2D A_1-π-A_2 copolymers was investigated by CV measurement. The cyclic voltammograms of copolymers are shown in Fig. 2. The results data of corresponding with CV curves are summarized in Table 2. As shown in Fig. 2, the oxidation onset potential (E_{ox}^{onset}) for P(DTPz-ID), P(dDTPz-ID), P(DTPz-DTBT) and P(dDTPz-DTBT) were 1.34 eV, 1.55 eV, 0.90 eV and 1.40 eV, respectively. The electrochemical equation ($E_{HOMO} = -4.8-(E_{ox}^{onset}-E_{1/2,ferrocene})$ and the half wave potential of ferrocene ($E_{1/2,ferrocene} = 0.55$ eV for A_1-A_2 polymers and 0.49 eV for A_1-π-A_2 polymers, respectively) allowed confirmation of a deep HOMO levels except P(DTPz-DTBT) of −5.65 eV, −5.86 eV, −5.15 eV and −5.71 eV for P(DTPz-ID), P(dDTPz-ID), P(DTPz-DTBT) and P(dDTPz-DTBT), respectively. Since air oxidation threshold is −5.20 eV, for a material to show oxidation stability, its HOMO level should be lower than that of the threshold [34]. HOMO levels of copolymers were 0.45 eV of P(DTPz-ID), 0.66 eV of P(dDTPz-ID), −0.05 eV of P(DTPz-DTBT) and 0.51 eV of P(dDTPz-DTBT), All polymers except P(DTPz-DTBT) of which are lower than −5.20 eV, which reflects their oxidation stability. Therefore, the devices introduced with P(DTPz-ID), P(dDTPz-ID) and P(dDTPz-DTBT) as donor polymer, which showed deep HOMO levels, are expected to have high open circuit voltage (V_{oc}) for PSCs.

The lowest occupied molecular orbital (LUMO) levels of copolymers were calculated by the difference in the E_g^{opt} between the HOMO levels, and were shown as −4.02 eV, −4.19 eV, −3.50 eV and −3.93 eV for P(DTPz-ID), P(dDTPz-ID), P(DTPz-DTBT) and P(dDTPz-DTBT), respectively. When the offset between LUMO levels of the copolymers and $PC_{71}BM$ acceptor (−4.20 eV) is more than the 0.3 eV or too low (below 0.2 eV), there would be insufficient driving force for efficient exciton dissociation at the polymer donor-fullerene acceptor interface, ensuring energetically favorable electron transfer [25,31]. The difference in LUMO levels between the copolymers of P(DTPz-ID), P(dDTPz-ID), P(DTPz-DTBT) and P(dDTPz-DTBT), and fullerene acceptors are 0.18 eV, 0.01 eV, 0.70 eV and 0.27 eV, respectively. Thus, P(DTPz-DTBT) and P(dDPz-DTBT) are expected to allow more efficient electron transfer compared to P(DTPz-ID) and P(dDTPz-ID) in active layer.

3.3. Theoretical calculations

In order to understand the electronic properties of the A_1-A_2 and 2D A_1-π-A_2 copolymers, DFT calculation was used to simulate the distribution of the electron density of states at repeating units (n), n = 1, 2 of copolymers in Fig. 3. To reduce computational time consumption, long alkyl side chains of copolymer backbones were simplified to methyloxy and isopropyl. The HOMO orbital of P(DTPz-ID) was delocalized in whole units, while case of P(dDTPz-ID) was localized in the D-thiophene unit including the DTPz, rather than delocalized on the entire main backbone (n = 1). This indicates that D-thiophene-DTPz unit works more as a donor than ID unit. The LUMO orbital of P(dDTPz-DTBT) also has totally localized in ID units, while those of P(DTPz-DTBT) localized in the entire units. The same results of HOMO and LUMO trends can be obtained for n = 2. Therefore similar electronic behavior can be expected in the polymers. HOMO and LUMO orbitals of P(DTPz-DTBT) also look like trends of P(DTPz-ID).

By comparing their distribution of electron density, P(dDTPz-DTBT) showed clear contrast to P(dDTPz-ID). When n = 1 for P(dDTPz-DTBT), HOMO levels were uniformly delocalized according to DTBT of D-thiophene unit including the DTPz and main backbone. This suggests P(dDTPz-DTBT) has more stable electronic distribution in HOMO levels compared to P(dDTPz-ID). In LUMO levels, P(dDTPz-DTBT) showed similar electron density to P(dDTPz-ID) and its electron clouds were localized in DTBT, which is stronger acceptor than DTPz. Same results were observed in n = 2, and thus the electronic behavior of P(dDTPz-DTBT) polymer is expected to differ to that of P(dDTPz-ID). Among the copolymers, the LUMO orbital has more electron clouds localized by ID acceptor cores other than the DTBT unit of D-thiophene. This suggests ID acceptor is more efficient at forming structural quinoid than DTBT acceptor, and thus have stronger electron withdrawing strength.

In n = 1, the calculated HOMO/LUMO energy levels of P(DTPz-ID), P(dDTPz-ID), P(DTPz-DTBT) and P(dDTPz-DTBT) were −5.07 eV/-2.70 eV, −4.91 eV/-2.73 eV, −4.81 eV/−2.53 eV and −4.75 eV/-2.54 eV, respectively. In n = 2, HOMO/LUMO energy

Table 2
Optical and electrochemical properties of polymers.

Polymer	UV–visible absorption			Cyclic voltammetry		
	Chloroform solution [nm]	Film [nm]	$E_g^{opt,a}$ [eV]	E_{ox}^{onset} [V]	HOMO[b] [eV]	LUMO[b] [eV]
	λ_{max} [nm]	λ_{max} [nm]				
P(DTPz-ID)	347, 416, 656	338, 666	1.63	1.40	−5.65	−4.02
P(dDTPz-ID)	319, 392, 619	341, 600	1.67	1.55	−5.86	−4.19
P(DTPz-DTBT)	342, 398, 581	405, 608	1.65	0.90	−5.15	−3.50
P(dDTPz-DTBT)	319, 392, 535	320, 396, 574	1.78	1.40	−5.71	−3.93

[a] Calculated from the intersection of the tangent on the low energetic edge of the absorption spectrum with the baseline.
[b] $E_{HOMO\ (or\ LUMO)} = -[E_{onset}(vs\ Ag/AgCl) - E_{1/2}(Fc/Fc^+\ vs\ Ag/AgCl)^c] - 4.8eV$.
[c] $E_{1/2}(Fc/Fc^+\ vs\ Ag/AgCl) = 0.55$ eV for A_1-A_2 polymers and 0.49 eV for for A_1-π-A_2 polymers (Measured data) [3,33].

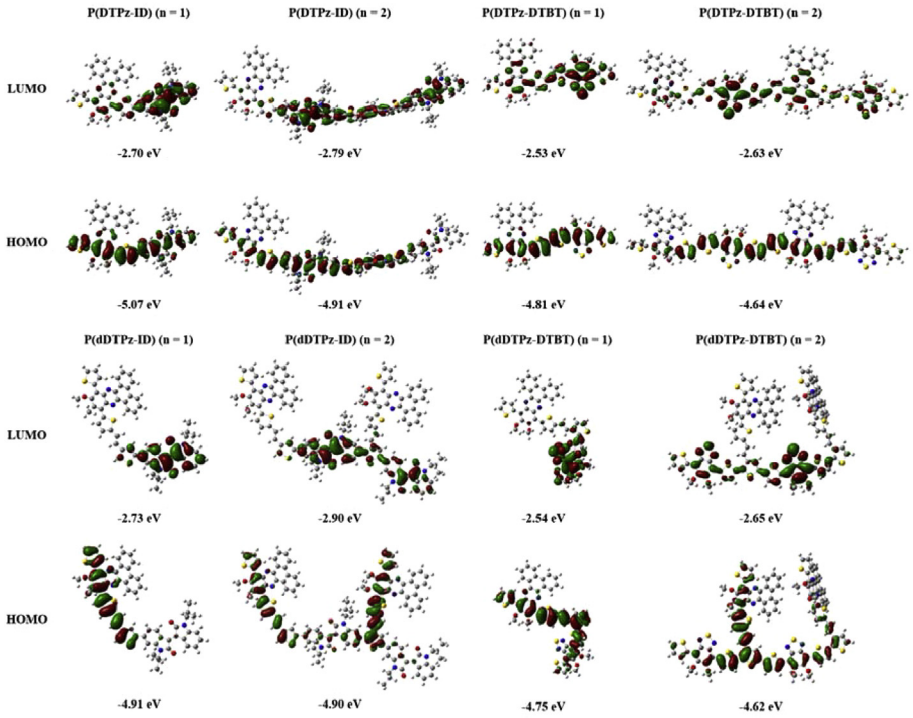

Fig. 3. DFT calculation data (HOMO & LUMO orbitals) of polymers (n = 1, 2).

levels of P(DTPz-ID), P(dDTPz-ID), P(DTPz-DTBT) and P(dDTPz-DTBT) were −4.91 eV/-2.79 eV, −4.90 eV/-2.90 eV, −4.64 eV/-2.63 eV and −4.62 eV/-2.65 eV, respectively. As the number of repeating units increase, P(DTPz-ID) and P(dDTPz-ID) showed localization of LUMO towards strong ID acceptor, P(DTPz-DTBT) and P(dDTPz-DTBT) showed localization of LUMO towards DTBT acceptor; LUMO energy levels of all polymers became increasingly deep. Specifically, in P(dDTPz-ID) where stronger acceptor, ID, than DTBT, was introduced, the offset in LUMO levels increased by 0.19 eV in n = 1 and by 0.25 eV in n = 2 compared to P(dDTPz-DTBT). Therefore, in polymerization, P(dDTPz-ID) is expected to have deeper-lying LUMO energy levels than P(dDTPz-DTBT).

Fig. 4 shows top view and side view of optimized geometries of conjugated backbones when A_1-A_2 and 2D A_1-π-A_2 copolymer is in n = 2. Fig. 5 shows the side view of the backbone to display calculated dihedral angles and dipole properties, and Table 3 is a summary of results on Fig. 5. Fig. 4 shows curvature of the main conjugated backbone for copolymers in blue line. As shown in Fig. 4, curvatures of P(DTPz-ID) and P(DTPz-DTBT) show straight-linear backbone, respectively, while P(dDTPz-ID) and P(dDTPz-DTBT) show curved-linear backbone, and planar and rigid structure along the blue line. This was clearly shown in calculated dihedral angles between units of each polymer, which is composed of main backbones. As shown in Fig. 5 and Table 3, dihedral angles (θ_1/θ_2) between alternating units in n = 2 for each polymer were calculated to be 21.1°/-19.3° for P(DTPz-ID), 25°/-38.9° for P(dDTPz-ID), 15.4°/-0.4° for P(dDTPz-DTBT) and 28.3°/-14.5° for P(dDTPz-DTBT). A_1-A_2 copolymers of P(DTPz-ID) and P(DTPz-DTBT) showed smaller dihedral angles compared to those of P(dDTPz-ID) and P(dDTPz-DTBT). As introduction rigid D-thiophene, 2D A_1-π-A_2 copolymers of P(dDTPz-ID) and P(dDtPz-DTBT) could be overlap of electron clouds due to big tilting relative to A_1-A_2 copolymers. This increases the electron-donating ability and results in the enhanced V_{oc} in fabricated devices [34]. Although θ_1 was 25° for P(dDTPz-ID), which is 3.3° lower tilting angle compared to θ_1 of P(dDTPz-DTBT), θ_2 was −38.9°, which is as much as 24.4° bigger tilting angle compared to θ_2 of P(dDTPz-DTBT). This suggests backbone curvature of P(dDTPz-DTBT) is planar compared to P(dDTPz-ID), and thus P(dDTPz-DTBT) in solid state is in advantage to have rigid backbone conformation [35,36].

Fig. 4 (a) and (b) show side chain directions of calculated polymer backbone for copolymers in red lines. The orientation of *N*-alkyl chains of ID that forms the main backbone of P(DTPz-ID) and P(dDTPz-ID) is symmetric, which is a contrast to the orientation of alkoxy chains of DTBT in P(DTPz-DTBT) and P(dDTPz-DTBT), which is asymmetric. Also, both polymers have alkoxy chains with D-thiophene-DTPz units in the main backbone in asymmetric orientation. Considering the overall findings, P(DTPz-ID) and P(dDTPz-ID) backbone had greater conformational disorder compared to P(DTPz-DTBT) and P(dDTPz-DTBT) was expected to have reduced stacking properties [37,38]. As shown in Fig. 5, in n = 2, the lengths of main polymer backbone ($L_{n=2}$) for P(DTPz-ID), P(dDTPz-ID), P(DTPz-DTBT) and P(dDTPz-DTBT) were calculated to be 42.72 Å, 27.21 Å, 47.46 Å and 29.64 Å, respectively. This shows that the length of main polymer chain of P(DTPz-DTBT) and P(dDTPz-DTBT) is longer than that of P(DTPz-ID) and P(dDTPz-ID) by 4.74 Å and 2.43 Å, respectively, and thus has increased probability of interchain packing of bulky fullerene derivative acceptors [39,40].

Gaussian calculation allowed calculation of strength and direction of dipoles in the all polymers. Dipole strength of P(DTPz-ID), P(dDTPz-ID), P(DTPz-DTBT) and P(dDTPz-DTBT) were calculated to be 2.38 D, 1.3 D, 3.56 D and 4.77 D, respectively. If net dipole orientation of copolymer-fullerene blend has the same with dipole direction of pristine polymer, P(dDTPz-DTBT) can have more enhanced charge transport compared to other polymers, and thus expected to have outstanding photovoltaic properties [41,42].

3.4. Photovoltaic properties

The optimized photovoltaic properties of the copolymers were evaluated by manufacturing PSC devices with an ITO/ZnO/polymer:$PC_{71}B$/MoO_3/Ag inverted structure. Fig. 6 shows (a) J-V curves

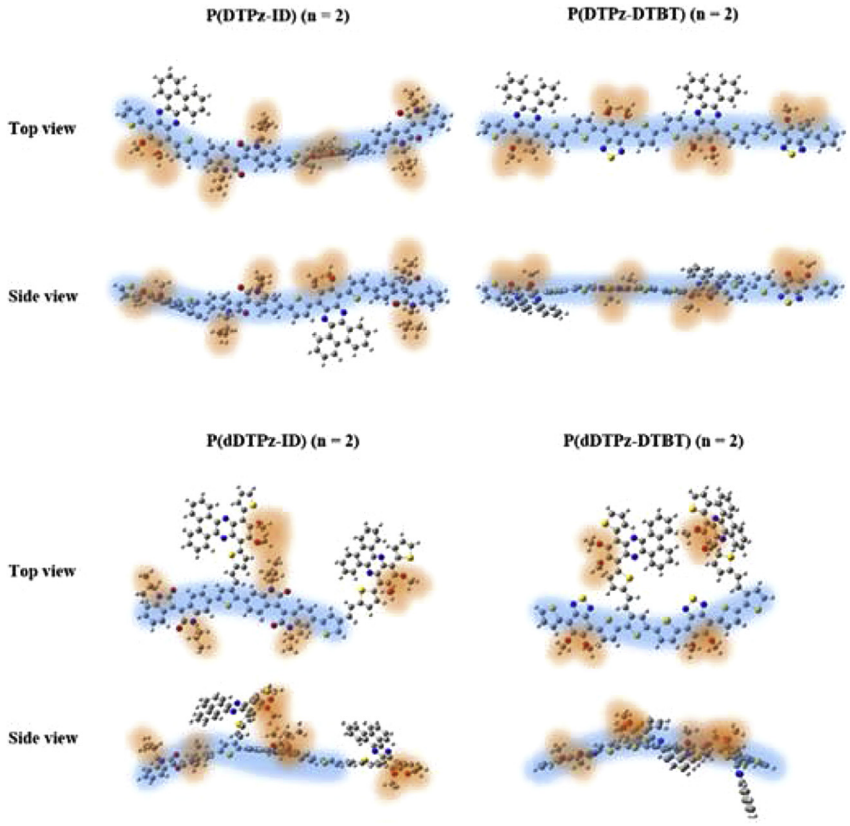

Fig. 4. Optimized geometries of polymer backbones (n = 2). in top view and side view.

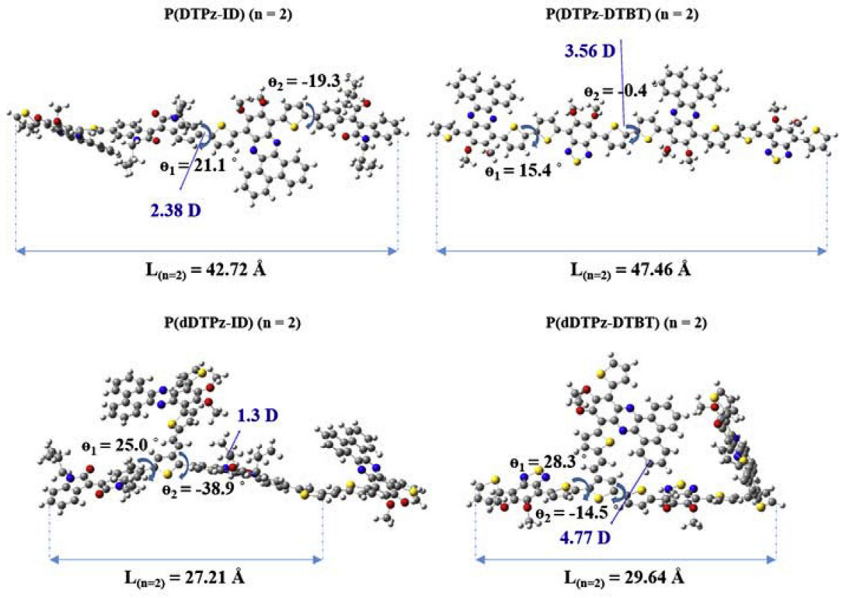

Fig. 5. Calculated dihedral angles, length and dipole properties of polymers (n = 2).

and (b) EQE curves of the results of PSC device for polymers. The photovoltaic performance for polymers are arranged in Table 4. As shown in Fig. 6 and Table 4, when P(DTPz-ID) and P(dDTPz-ID) blended to $PC_{71}BM$ in 1:1.5 and 1:3 ratio in optimized condition of 1.0 wt% concentration of CB with 1.0% DIO, it displayed 0.3% and 0.4% of PCE with 0.859 V and 0.95 V of V_{oc}, same 1.2 mA/cm^2 of short-circuit current density (J_{sc}), and 30.4% amd 38.0% of FF at 80 nm of thickness, respectively. On the other hand, P(DTPz-DTBT) and P(dDTPz-DTBT) in the same optimized conditions showed 5.0% of the best PCE with 0.596 V and 1.0 V of V_{oc} and 7.1 mA/cm^2 and 11.4 mA/cm^2 of J_{sc}, and 43.1% and 43.2% of FF at 100 nm of thickness, respectively (see Table 4).

Table 3
Calculated dihedral angles, length and dipole moment of polymers through Gaussian.

polymer	θ_1 (°)	θ_2 (°)	Length of main backbone (n = 2) (Å)	Dipole moment (D)
P(DTPz-ID)	21.1	−19.3	42.72	2.38
P(dDTPz-ID)	25.0	−38.9	27.21	1.3
P(DTPz-DTBT)	15.4	−0.4	47.46	3.56
P(dDTPz-DTBT)	28.3	−14.5	29.64	4.77

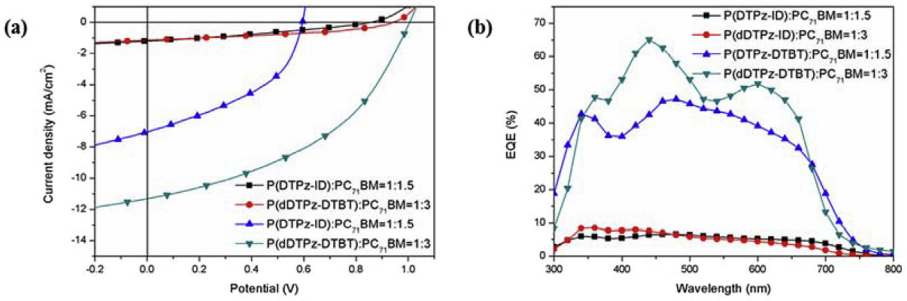

Fig. 6. (a) J-V curves and (b) EQE curves of the optimized solar cell devices for polymers.

Table 4
Photovoltaic performances of polymers.

polymer:$PC_{71}BM$ blend	V_{oc} [V]	J_{sc} [mA/cm^2]	J_{sc}^{cal} [mA/cm^2]	FF [%]	PCE [%]	EQE_{max} [%]
P(DTPz-ID), 1:1.5	0.859	1.2	1.2	30.4	0.3	6.6 (460 nm)
P(dDTPz-ID), 1:3	0.955	1.2	1.1	38.0	0.4	8.5 (360 nm)
P(DTPz-DTBT), 1:1.5	0.596	7.1	8.4	43.1	1.8	47.2 (480 nm)
P(dDTPz-DTBT), 1:3	1.00	11.4	10.6	43.2	5.0	65.0 (440 nm)

Both polymers of P(dDTPz-ID) and P(dDTPz-DTBT) with 2D A_1-π-A_2 structure had very high V_{oc} of 0.955–1.0 V compared to those of P(DTPz-ID) and P(DTPz-DTBT). This is the result of the difference between deep HOMO levels of copolymers and LUMO level of $PC_{71}BM$ [43]. However, J_{sc} of P(DTPz-ID) and P(dDTPz-ID) was measured to be 1.2 mA/cm^2 which was significantly lower compared to P(DTPz-DTBT) and P(dDTPz-DTBT). This is due to extremely deep-lying LUMO level of −4.02 eV and −4.19 eV, resulting in 0.18 eV and 0.01 eV difference with $PC_{71}BM$ LUMO level of −4.20 eV, which led to insufficient driving force, resulting in simultaneous charge separation and charge recombination [44]. As shown in Fig. 6 (b), P(DTPz-DTBT) and P(dDTPz-DTBT) UV–visible absorption spectra show uniform 40–65% external quantum efficiency (EQE) (EQE_{max} = 47.2% and 65.0%) in all absorption range, while P(DTPz-ID) and P(dDTPz-ID) EQE show lower than 10% efficiency (EQE_{max} = 6.5%, 8.5%), respectively. This reflects the fact that produced charge carriers are not effectively separated and transported in P(DTPz-ID) or P(dDTPz-ID)-$PC_{71}BM$ network, respectively [45]. FF values of all polymers showed similar results of around 40%. Low FFs of copolymers are generally caused by high series resistances (R_s), that is 6890 Ω, 909.56 Ω, 395.92 Ω and 300.96 Ω for P(DTPz-ID), P(dTPz-ID), P(DTPz-DTBT) and P(dDTPz-DTBT), respectively. According to overall device data, when A_1-π is D-thiophene-DTPz unit and A_2 is DTBT, in the A_1-π-A_2 building block, efficiency of PSCs increased.

3.5. XRD analysis

To investigate the interchain packing structures of pristine and blend films for copolymers, we also conducted XRD analysis. Fig. 7 (a) and (b) show out-of-plane and (c) and (d) show in-plane mode measurements of XRD patterns of pristine and $PC_{71}BM$ blend films for P(DTPz-ID), P(dDTPz-ID), P(DTPz-DTBT) and P(dDTPz-DTBT). In the out-of-plane measurements, pristine film for P(DTPz-ID) and P(dDTPz-ID) showed lamellar packing peak of (100) plane in 3.7° and 4° for 2θ, respectively. Calculation using Bragg's law ($\lambda = 2d\sin\theta$) to substitute 2θ confirmed lamellar packing d-spacing (d_1) with and 23.88 Å and 22.09 Å for P(DTPz-ID) and P(dDTPz-ID), respectively. On the other hand, for P(DTPz-DTBT) and P(dDTPz-DTBT), no peak was observed for lamellar packing. All polymers showed π-π stacking peaks that represent (010) plane in 21.35°, 20.55°, 21.30° and 22.12°, respectively. Calculation using Bragg's law on the π-π stacking distances (d_π) of copolymers resulted in 4.16 Å, 4.32 Å, 4.17 Å and 4.02 Å, respectively. This shows that in pristine films, P(dDTPz-DTBT) copolymer chain on the substrate would have 0.14–0.3 Å closer face-on orientation than the other polymers and are stacked. Also, as shown in Fig. 7 (b) in-plane mode, P(dDTPz-DTBT) showed (100) peak, which suggests that it has predominant face-on structure compared to P(dDTPz-ID).

Next, stacking properties of copolymer chains for copolymers with increasing $PC_{71}BM$ inter-chain packing were observed. As shown in Fig. 7 (a) out-of-plane, $PC_{71}BM$ blend films for P(DTPz-ID), P(dDTPz-ID), P(DTPz-DTBT) and P(dDTPz-DTBT) both showed enhanced face-on structure than pristine films as $PC_{71}BM$ was packed closer between polymer chain. In P(DTPz-ID) and P(dDTPz-ID), lamellar peak near 3.7° and 4° disappeared and only π-π stacking peak was observed at 26.15° and 26.4°, respectively. Bragg's law calculation result was 3.41 Å and 3.38 Å, which suggests closer packing by 0.75–0.94 Å compared to pristine films, respectively. In P(DTPz-DTBT) and P(dDTPz-DTBT), π-π stacking distance was 3.62 Å and 3.31 Å, which is 0.55–0.71 Å closer. (Both polymers showed $PC_{71}BM$ peak near 19°.) These results suggest synthesized A_1-π-A_2 building blocks have beneficial structures for $PC_{71}BM$ inter-chain packing (See Table 5).

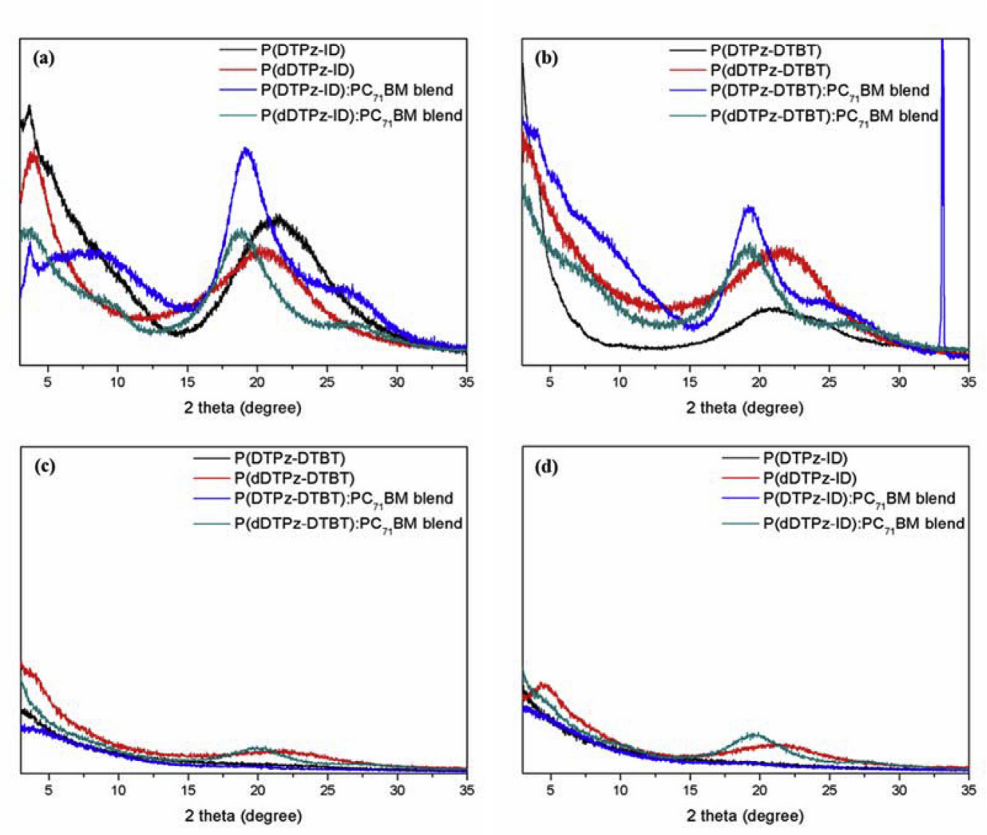

Fig. 7. XRD profiles of pristine polymer films and polymer:$PC_{71}BM$ blend films on silicon wafer (a, b) out-of-plane and (b, c) in-plane mode. (For interpretation of the references to colour in this figure legend, the reader is referred to the Web version of this article.)

Table 5
XRD data of polymers.

Polymer	Conditions	2-theta [°]/d_{100} [Å]	2-theta [°]/d_{PC71BM} [Å]	2-theta [°]/d_{010} [Å]
P(DTPz-ID)	*Pristine*	3.7/23.9	–	21.35/4.16
	with $PC_{71}BM$	–	19.10/4.65	26.15/3.41
P(dDTPz-ID)	*Pristine*	4.0/22.12	–	20.55/4.32
	with $PC_{71}BM$	–	18.86/4.70	26.40/3.38
P(DTPz-DTBT)	*Pristine*	–	–	21.30/4.17
	with $PC_{71}BM$	–	19.17/4.63	24.60/3.62
P(dDTPz-DTBT)	*Pristine*	–	–	22.12/4.02
	with $PC_{71}BM$	–	19.32/4.59	26.90/3.31

3.6. Morphology and hole mobility analysis

The surface morphology of the optimized polymer:$PC_{71}BM$ blends are a crucial factor that determines the efficiency of PSCs, and thus obtaining fine morphology is essential. As is well-known, the fine morphology of the blend films should include an ideal domain size of 10–20 nm of polymer and fullerene with an interpenetrating bi-continuous network, and both smaller (<10–20 nm) and larger (>10–20 nm) domain sizes of the blend films will limit charge transfer and separation [46]. Therefore, the nanoscale morphologies of optimized blend films for copolymers were examined by tapping mode AFM in Fig. 8. As shown in 2D and 3D topography in Fig. 8 (a) and (b), as $PC_{71}BM$ is packed into P(DTPz-ID) and P(dDTPz-ID), microscale morphology showed smooth and uniform morphology with low root-mean-square (RMS) roughness of 0.104 and 0.454, respectively. However, nanoscale morphology showed PCBM dark clusters across the film and partial phase aggregation. This is due to poor miscibility of the polymer and $PC_{71}BM$ which leads to increase in charge recombination at the D-A interface to reduce FF, thus PCE is decreased [22].

On the other hand, as shown in 2D and 3D topography in Fig. 8 (c) and (d), P(DTPz-DTBT) and P(dDTPz-DTBT) blended with $PC_{71}BM$ were smoother than copolymers:$PC_{71}BM$ blend based on ID unit, and formed fiber-like small size domain and had homogeneous morphology with 0.570 nm and 0.566 nm, respectively [30]. P(dDTPz-DTBT) films showed better morphology in D-A segregation compared to those of P(DTPz-DTBT). This is due to good miscibility of P(dDTPz-DTBT) and $PC_{71}BM$; interpenetrating D-A networks was formed to allow efficient charge transfer and separation. However, the devices based on the both polymers blended with $PC_{71}BM$ still showed the low FF.

The charge carriers transport properties of conjugated polymers play role in the performance of PSCs. To understand the influence of hole mobility of the copolymers is measured by the space charge limited current (SCLC) method in the hole-only devices with a device structure of ITO/PEDOT:PSS/Polymer:$PC_{71}BM$/MoO_3/Ag, and

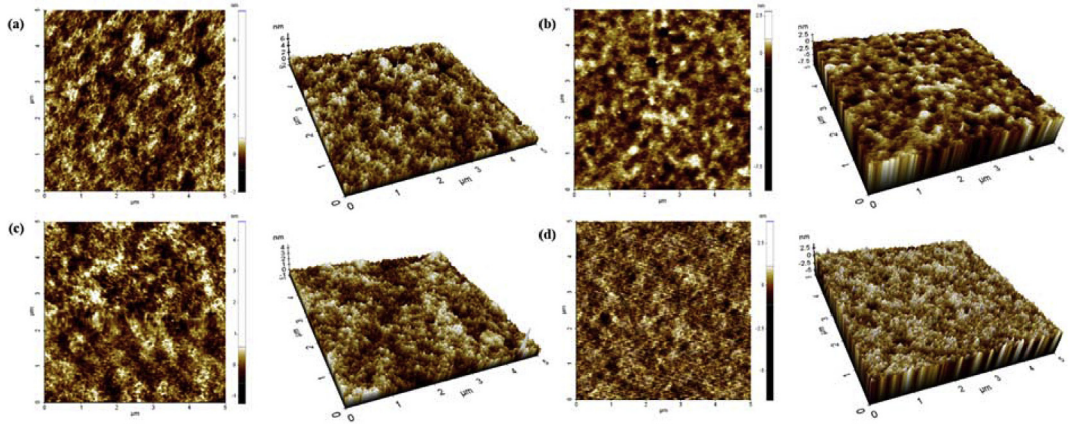

Fig. 8. AFM images of the optimized polymer:$PC_{71}BM$ blend films (a) P(DTPz-ID):$PC_{71}BM$ = 1:1.5, (b) P(dDTPz-ID):$PC_{71}BM$ = 1:3, (c) P(DTPz-DTBT):$PC_{71}BM$ = 1:1.5, and (d) P(dDTPz-DTBT):$PC_{71}BM$ = 1:3.

the Poole-Frenkel Law SCLC formula {eqn. $J = (9/8)\varepsilon_0\varepsilon_r\mu(V\text{-}V_{bi})^2/(L^3)\exp 0.89\gamma[(V\text{-}bi)/L]^{0.5}$ where J is the current density, μ is the charge carrier mobility, ε_0 is the permittivity of free space (8.85×10^{-14} F cm^{-1}), ε_r is the relative permittivity of the material (assumed to be 3), L is the thickness of the active layer (80–100 nm), and V is the effective voltage.}was used to calculate the hole mobility.

The results are plotted as $\ln(JL^3/V^2)$ vs. $(V/L)^{0.5}$, as shown in Fig. S12. According to eqn., the hole mobilities of 7.68×10^{-8} cm^2 V^{-1} s^{-1}, 8.19×10^{-8} cm^2 V^{-1} s^{-1}, 8.95×10^{-6} cm^2 V^{-1} s^{-1} and 7.33×10^{-6} cm^2 V^{-1} s^{-1} are observed for P(DTPz-ID), P(dDTPz-ID), P(DTPz-DTBT) and P(dDTPz-DTBT), respectively. In particular, P(dDTPz-DTBT) has a highest hole mobility, which is two orders higher than those of P(dDTPz-ID). The results clearly explain the J_{sc} trend of the copolymers. Simultaneously, the unbalanced charge carrier mobilities between the hole mobility of copolymers and electron mobility of $PC_{71}BM$ (1×10^{-4} cm^2 V^{-1} s^{-1}) also explain the reason for low FF values of the devices [46–49].

4. Conclusion

In this study, two new types of 2D A_1-π-A_2 copolymers for P(dDTPz-ID) and P(dDTPz-DTBT) were designed and synthesized based on the DTPz as A_1 acceptor, ID and DTBT as more strong A_2 acceptors than A_1. Two copolymers displayed a benefit of A-A building blocks, which is complementary and broad light absorption from 300 to 750 nm due to acceptors with different withdrawing strengths. Also, the introduction of D-thiophene unit allowed the formation of 2D-strcuture, which led to effective interchain packing of $PC_{71}BM$ for both copolymers. Also, it exhibited enhanced π-π stacking properties compared to polymer-$PC_{71}BM$ blends and had predominant face-on structure, which was confirmed by XRD. The optimized devices for P(dDTPz-ID) showed 0.4% PCE. The low efficiency of P(dDTPz-ID) is due to low J_{sc}. The main reason for low J_{sc} is that the LUMO level of the polymer (−4.19 eV) did not correspond well with the level of $PC_{71}BM$ (−4.20 eV), affecting charge transport. On the other hand, optimized device for P(dDTPz-DTBT) showed efficient charge transport from enhanced energy alignment, high V_{oc} and dipole moment and fine morphology compared to P(dDTPz-ID), and thus obtained 11.4 mA/cm^2 of J_{sc} with 5.0% of best PCE. The study in this work provide a new possibility for molecular design of 2D A_1-π-A_2 copolymers in PSCs [19].

Acknowledgements

This research was supported by the New & Renewable Energy Core Technology Program (No. 20153010140030) and Human Resources Program in Energy Technology (No. 20174010201540) of the Korea Institute of Energy Technology Evaluation and Planning grant funded by the Ministry of Trade, industry & Energy, Republic of Korea.

Appendix A. Supplementary data

Supplementary data related to this article can be found at https://doi.org/10.1016/j.polymer.2018.04.032.

References

[1] V. Shrotriya, Nat. Photon. 3 (2009) 447–449.
[2] L. Lan, Z. Chen, Q. Hu, L. Ying, R. Zhu, F. Liu, T.P. Russell, F. Huang, Y. Cao, Adv. Sci. 3 (2016) 1600032.
[3] T.H. Lee, M.H. Choi, S.J. Jeon, D.K. Moon, Polymer 99 (2016) 756–766.
[4] L. Lu, T. Zheng, Q. Wu, A.M. Schneider, D. Zhao, L. Yu, Chem. Rev. 115 (2015) 12666–12731.
[5] N.C. Cates, R. Gysel, Z. Beiley, C.E. Miller, M.F. Toney, M. Heeney, I. Mcculloch, M.D. Mcgehee, Nano Lett. 9 (12) (2009) 4153–4157.
[6] T. Xiao, H. Xu, G. Grancini, J. Mai, A. Petrozza, U.S. Jeng, Y. Wang, X. Xin, Y. Lu, N.S. Choon, H. Xiao, B.S. Ong, X. Lu, N. Zhao, Sci. Rep. 4 (2014) 17–19.
[7] W. Zhuang, A. Lundin, M.R. Andersson, J. Mater. Chem. 2 (2014) 2202–2212.
[8] Z. Zeng, Z. Zhang, B. Zhao, H. Liu, X. Sun, G. Wang, J. Zhang, S. Tan, J. Mater. Chem. 5 (2017) 7300–7304.
[9] D. Mo, H. Wang, H. Chen, S. Qu, P. Chao, Z. Yang, L. Tian, Y.-A. Su, Y. Gao, B. Yang, W. Chen, F. He, Chem. Mater. 29 (2017) 2819–2830.
[10] J. Yuan, L. Qiu, Z.G. Zhang, Y. Li, Y. Chen, Y. Zou, Nanomater. Energy 30 (2016) 312–320.
[11] S. Xu, L. Feng, J. Yuan, Z.G. Zhang, Y. Li, H. Peng, Y. Zou, ACS Appl. Mater. Interfaces 9 (2017) 18816–18825.
[12] Q. Tu, D. Cai, L. Wang, J. Wei, Q. Shang, S. Chen, Y. Ma, Z. Yin, C. Tang, Q. Zheng, J. Mater. Chem. C 4 (2016) 6160–6168.
[13] J. Fan, Y. Zhang, C. Lang, M. Qiu, J. Song, R. Yang, F. Guo, Q. Yu, J. Wang, L. Zhao, Polymer 82 (2016) 228–237.
[14] N. Xiao, L. Qian, J. Cao, X. Zhao, A. Han, L. Ding, New J. Chem. 40 (2016) 4895–4898.
[15] R. Kroon, A. Diaz, D.Z. Mendaza, S. Himmelberger, J. Bergqvist, F. Gao, A. Obaid, W. Zhuang, D. Gedefaw, E. Olsson, A. Salleo, M.R. Andersson, J. Am. Chem. Soc. 136 (2014) 11578–11581.
[16] J. Zhao, Y. Li, A. Hunt, J. Zhang, H. Yao, Z. Li, J. Zhang, F. Huang, H. Ade, H. Yan, Adv. Mater. 28 (2016) 1868–1873.
[17] M. Zhang, X. Guo, W. Ma, H. Ade, J. Hou, Adv. Mater 56 (2014) 5880–5885.
[18] Y. Liu, J. Zhao, Z. Li, C. Mu, W. Ma, H. Hu, K. Jiang, H. Lin, H. Ade, H. Yan, Nat. Commun. 5 (5) (2014) 1–8.
[19] Y. Chao, J. Jheng, J. Wu, K. Wu, H. Peng, M. Tsai, C. Wang, Y. Hsiao, C. Wang, C. Lin, C. Hsu, 26, (2014) 5205–5210.
[20] P. Shen, H. Bin, L. Xiao, Y. Li, Macromolecules 46 (2013) 9575–9586.
[21] X. Xu, K. Feng, K. Li, Q. Peng, J. Mater. Chem. 3 (2015) 23149–23161.
[22] X. Liu, F. Wu, H. Guo, B. Zhao, S. Tan, eXPRESS Polymer Lett. 9 (11) (2015)

1027–1039.
[23] Z. Li, Y. Zhang, S. Tsang, X. Du, J. Zhou, Y. Tao, J. Ding, J. Phys. Chem. C 115 (2011) 18002–18009.
[24] Q. Tao, Y. Xia, X. Xu, S. Hedstro, O. Ba, D.I. James, L. Hou, W. Zhu, E. Wang, Macromolecules 48 (2015) 1009–1016.
[25] H.J. Cho, Y.J. Kim, S. Chen, J. Lee, T.J. Shin, C.E. Park, C. Yang, Nanomater. Energy 39 (2017) 229–237.
[26] W. Sun, Z. Ma, D. Dang, W. Zhu, M.R. Andersson, F. Zhang, E. Wang, J. Mater. Chem. 1 (2013) 11141–11144.
[27] M. Liu, Y. Gao, Y. Zhang, Z. Liu, L. Zhao, Polym. Chem. 8 (2017) 4613–4636.
[28] H.J. Song, J.Y. Lee, E.J. Lee, D.K. Moon, Eur. Polym. J. 49 (2013) 3261–3270.
[29] M. Choi, K.W. Song, D.K. Moon, Polym. Chem. 6 (2015) 2636–2646.
[30] Z. Gu, L. Deng, H. Luo, X. Guo, H. Li, Z. Cao, X. Liu, X. Li, H. Huang, Y. Tan, Y. Pei, S. Tan, J. Polym. Sci. Part a : Polym. Chem. 50 (2012) 3848–3858.
[31] H. Li, H. Luo, Z. Cao, Z. Gu, P. Shen, H. Che, G. Yu, S. Tan, J. Mater. Chem. 22 (2012) 22913–22921.
[32] H. Tan, X. Deng, J. Yu, B. Zhao, Y. Wang, Y. Liu, W. Zhu, H. Wu, Y. Cao, Macromolecules 46 (2013) 113–118.
[33] M. Choi, T.H. Lee, Y.W. Han, D.K. Moon, J. Polym. Sci. Part a Polym. Chem. 54 (2016) 2746–2759.
[34] J. Lee, H. Ko, E. Song, H.G. Kim, K. Cho, ACS Appl. Mater. Interfaces 7 (2015) 21159–21169.
[35] H. Li, X. Zheng, X. Wang, F. Liu, H. Fu, Polym. Chem. 6 (2015) 6637–6643.
[36] C. Huang, S. Wu, Y. Huang, Y. Chen, S. Chang, T. Wu, K. Wu, W. Chuang, C. Wang, Chem. Mater. 28 (2016) 5175–5190.
[37] I. Constantinou, T. Lai, E.D. Klump, S. Goswami, K.S. Schanze, F. So, ACS Appl. Mater. Interfaces 7 (2015) 26999–27005.
[38] N.C. Miller, E. Cho, R. Gysel, C. Risko, V. Coropceanu, C.E. Miller, S. Sweetnam, A. Sellinger, M. Heeney, I. Mcculloch, J. Brédas, M.F. Toney, M.D. Mcgehee, Adv. Energy Mater 2 (2012) 1208–1217.
[39] T. Wang, A.J. Pearson, D.G. Lidzey, J. Mater. Chem. C 1 (2013) 7266–7293.
[40] L. Chen, X. Liu, Y. Wei, F. Wu, Y. Chen, Phys. Chem. Chem. Phys. 18 (2015) 2219–2229.
[41] B. Carsten, J.M. Szarko, H.J. Son, W. Wang, L. Lu, F. He, B.S. Rolczynski, S.J. Lou, L.X. Chen, L. Yu, J. Am. Chem. Soc. 133 (2011) 20468–20475.
[42] P.P. Boix, M.M. Wienk, R.A.J. Janssen, G. Garcia-Belmonte, J. Phys. Chem. 115 (2011) 15075–15080.
[43] T. Kumair, S.M. Lee, S. Kang, S. Chen, C. Yang, Energy Environ. Sci. 10 (2017) 258–265.
[44] M. Zhang, F. Wu, Z. Cao, T. Shen, H. Chen, X. Li, S. Tan, Polym. Chem. 5 (2014) 4054–4060.
[45] K.H. Park, Y. An, S. Jung, H. Park, C. Yang, ACS Nano 11 (2017) 7409–7415.
[46] B. Qiu, R. Cui, J. Yuan, H. Peng, Z. Zhang, Y. Li, Y. Zou, Phys. Chem. Chem. Phys. 17 (2015) 17592–17600.
[47] T. Jiang, J. Yang, Y. Tao, C. Fan, L. Xue, Z. Zhang, H. Li, Y. Li, W. Huang, Polym. Chem. 7 (2016) 926–932.
[48] M. Jeong, S. Chen, S.M. Lee, Z. Wang, Y. Yang, Z. Zhang, C. Zhang, M. Xiao, Y. Li, C. Yang, Adv. Energy Mater 8 (2018) 1702166.
[49] S. Kang, T. Kumari, S.M. Lee, M.J.,C. Yang, Adv. Energy Mater 7 (2017) 1700349.